Appendix A from L. T. Burghardt et al., "Modeling the Influence of Genetic and Environmental Variation on the Expression of Plant Life Cycles across Landscapes"

Phenology and Environmental Model Details

Germination Submodel

Temperature and moisture are major seasonal factors that determine germination timing in combination with the depth of primary dormancy (Gutierrez et al. 2007; Holdsworth et al. 2008; Graeber et al. 2012). To project the timing of germination, we used a hydrothermal germination submodel that incorporates both dormancy variation within cohorts (Alvarado and Bradford 2002) and a function describing the rate of primary dormancy loss (Bair et al. 2006). In the hydrothermal submodel, progress toward germination is a function of hourly soil temperature, moisture level, and dormancy level that reduces germination progress (Finch-Savage and Leubner-Metzger 2006; Batlla and Benech-Arnold 2010). Each hour, cumulative progress toward germination is summed until the germination threshold is reached. In general, germination progress is faster at higher temperatures and higher moisture levels (up to the optimum temperature and saturation point, respectively). Hydrothermal models perform well in field conditions, particularly for the earliest 70% of germinants (Hardegree and Van Vactor 1999; Meyer and Allen 2009).

A standard feature of many germination models, strongly supported by empirical studies of *Arabidopsis thaliana*, is that genetically identical offspring start life with a distribution of initial dormancy levels (Bradford 2002; Finch-Savage and Leubner-Metzger 2006; Hardegree 2006). We model the primary dormancy distribution of offspring as being determined by maternal parameters (genotype) and insensitive to maternal environment. By explicitly modeling this variation, we incorporate a ubiquitous phenomenon known to occur in *A. thaliana* and many other species. Traditional germination models use the population of seeds as the unit of analysis. Our approach differs in that we track the behavior of individual seeds. This formulation does little to change the quantitative results but has many practical advantages. For instance, variation in initial primary seed dormancy may be defined according to any state distribution. Most importantly, it allows us to keep track of individual seed fates across generations.

Hydrothermal models are based on empirical observations that hold across many species: (1) in response to lower moisture levels during imbibition, fewer seeds germinate and they do so at a slower rate; (2) seeds within a population do not all respond to moisture conditions in the same way; and (3) germination rates increase up to an optimum temperature and subsequently decline. These observations suggest that each seed has a base water potential (Ψ_b), analogous to a base temperature, below which it cannot make progress toward germination. During germination at suboptimal temperatures, seeds generally maintain the same base moisture for germination (Ψ_b) regardless of temperature; but at supraoptimal germination conditions, the base moisture level (Ψ_b) increases with increasing temperature, slowing germination rate. The following equation formalizes these observations, allowing computation of the hydrothermal units accrued toward germination each hour ($\mathrm{HTU}_{\mathrm{germ}}(\tau)$; adapted from Alvarado and Bradford 2002):

$$\mathrm{HTU}_{\mathrm{germ}}(\tau) = \begin{cases} (\Psi(\tau) - \Psi_b(\tau)) \times (T(\tau) - T_{b.g}) & \text{when } T_{b.g} < T(\tau) \leq T_o \text{ and } \Psi_b(\tau) < \Psi(\tau) \text{ and} \\ (\Psi(\tau) - m\Psi_b(\tau)) \times (T_o - T_{b.g}) & \text{when } T(\tau) > T_o \text{ and } m\Psi_b(\tau) < \Psi(\tau) \\ 0 & \text{otherwise} \end{cases}.$$

The first function is used at suboptimal temperatures, and the second function is used at supraoptimal temperatures. Values T and Ψ are temperature (°C) and moisture (in MPa) during a given hour (τ), respectively. Value T_o is the optimal temperature for germination (that which maximizes the germination rate), and $T_{b.g}$ is a constant parameter indicating the temperature below which no progress toward germination occurs. Analogously, Ψ_b is the base moisture level of a particular seed below which no progress toward germination occurs.

At supraoptimal temperatures, the Ψ_b of a seed is modified based on how much the current temperature is above the optimum temperature, according to

$$m\Psi_b(\tau) = \Psi_b(\tau) + k_T(T(\tau) - T_o).$$

Here k_T is an empirically derived scalar that defines the shift in Ψ_b for each degree the current temperature is above the

optimal temperature. We estimated k_T from a batch of afterripened Columbia seeds (L. T. Burghardt, unpublished data) by measuring germination across a range of high temperatures.

Germination progress is summed together each hour from dispersal ($\tau_{\text{dispersal}}$) to provide a cumulative measure of germination progress (germ_{sum}). When the germination threshold (Θ_{germ}) is reached, the germination transition occurs:

$$\text{germ}_{\text{sum}}(\tau_{\text{dispersal}}) = \sum_{\tau_{\text{dispersal}}=0}^{\text{germ}_{\text{sum}}(\tau_{\text{dispersal}})=\Theta_{\text{germ}}} \text{HTU}_{\text{germ}}(\tau).$$

We compared the predictions of the standard hydrothermal germination model with parameters derived from the *A. thaliana* literature to a batch of Columbia seeds that were 19 weeks old and matured at 20°C (fig. A1). At this age, seeds have lost most of their primary dormancy. In our model, there is a minimum dormancy level (Ψ_{min}, set to -1), and therefore as primary dormancy is lost, Ψ_b values in a seed cohort start to pile up at -1, leading to a skewed dormancy distribution. Therefore, we used a Poisson distribution as an estimate of the dormancy distribution at this age (fig. A1*a*). Figure A1*b* shows our predictions superimposed on the experimentally measured germination times. Note that the current model consistently overestimates time to germination for Columbia seeds at cool temperatures, but the standard model is not flexible enough to accommodate this pattern. Interestingly, these predictions at cold temperatures are a much better match to the germination behavior of another German ecotype, Landsberg.

In *A. thaliana* and many other species, dormancy levels change with age via a process called afterripening (Carrera et al. 2007; Finch-Savage et al. 2007; Iglesias-Fernández et al. 2011). This process is rarely incorporated in germination models (for exceptions, see Batlla and Benech-Arnold 2003; Chantre et al. 2010). We combined the germination model above with a primary dormancy loss function originally developed for *Bromus tectorum* (Bair et al. 2006; Meyer and Allen 2009). In the hydrothermal germination model outlined above, the base water potential (Ψ_b) of the seed modifies the developmental rate and is therefore considered a measure of the dormancy level of the seed (Bradford 2002; Batlla and Benech-Arnold 2010). If Ψ_b is above 0, no progress toward germination can be made in any environmental condition. Empirical data demonstrate that Ψ_b values for a population of seeds decreases as primary dormancy is lost, and this is also true in *A. thaliana* (Footitt et al. 2011; L. T. Burghardt, unpublished data).

Afterripening models describe mathematically how Ψ_b changes over time after seeds are shed. We model the process of afterripening (primary dormancy loss) as a gradual, unidirectional loss of dormancy, with the rate of dormancy loss dependent on hourly soil surface temperature $T(\tau)$ and moisture $\Psi(\tau)$ conditions. This model was created for *Bromus tectorum* because there are little data available for *A. thaliana*. As described in the following equation, each hour the amount of afterripening time accrued is calculated and added to the running sum of the afterripening (AR_{sum}) experienced since seed dispersal:

$$\text{AR}_{\text{sum}}(\tau+1) = \begin{cases} \text{AR}_{\text{sum}}(\tau) + T(\tau) - T_{\text{b.ar}} & \text{when } \Psi_{\text{max}} \geq \Psi(\tau) \geq \Psi_u \\ \text{AR}_{\text{sum}}(\tau) + \dfrac{\Psi_l - \Psi(\tau)}{(\Psi_l - \Psi_u)}(T(\tau) - T_{\text{b.ar}}) & \text{when } \Psi_l < \Psi(\tau) < \Psi_u \\ \text{AR}_{\text{sum}}(\tau) & \text{when } \Psi(\tau) \leq \Psi_{\text{max}} \text{ or } \Psi(\tau) \leq \Psi_l \end{cases}.$$

Here Ψ_l is the lower moisture limit below which no afterripening occurs, and Ψ_u is the moisture level at which afterripening effectiveness levels off. In response to temperatures rising above the base temperature for afterripening ($T_{\text{b.ar}}$), the afterripening rate increases linearly. In response to moisture, the afterripening rate follows a broken stick model, such that at extremely low moisture, no afterripening occurs; above that, the rate increases linearly up until a saturation point (Ψ_u). High temperatures in moist conditions are the most effective at promoting afterripening. Afterripening does not occur in extremely moist conditions ($>\Psi_{\text{max}}$). This model is taken directly from Bair et al. (2006) and has not been fit directly for *A. thaliana*.

Next, we used the number of days (d_{sat}) it takes seeds to go from 0 Ψ_b to -1 Ψ_b under lab storage—room temperature (20°C) and dry (<-200 MPa)—conditions and the equation above to calculate the cumulative afterripening that occurred over that time period. Because the model works in hours not days, d_{sat} is multiplied by 24.

To determine the proportion of afterripening completed and the current seed dormancy level (Ψ_b), the current cumulative afterripening sum is divided by a cumulative afterripening sum that leads to a known amount of dormancy loss in the lab:

$$\Psi_b(\tau) = \begin{cases} \max\left(\Psi_i - \Psi_{\text{scale}} \dfrac{\text{AR}_{\text{sum}}(\tau)}{\text{AR}_{\text{sum}}(\text{lab conditions}) \times d_{\text{sat}} \times 24}, \Psi_{\text{min}}\right) & \text{if } \Psi_b(\tau) > \Psi_{\text{min}} \\ \Psi_{\text{min}} & \text{if } \Psi_b(\tau) \leq \Psi_{\text{min}} \end{cases}.$$

Seed dormancy Ψ_b at time (τ) is calculated by subtracting the amount of accumulated afterripening from the initial dormancy level (Ψ_i) of the seed and is incrementally modified hourly until the seed reaches an empirically approximated minimum dormant state (Ψ_{min}). We assume that all seeds can reach this minimum dormancy level after enough time. Minimum dormant state Ψ_{min} was estimated for Columbia seeds stored in lab conditions by determining how long it took for most seeds to germinate uniformly at a Ψ_b value near the estimated Ψ_{min}.

Flowering Submodel

In *Arabidopsis thaliana*, high temperature and long photoperiods are the major environmental factors that promote flowering (Mitchell-Olds and Schmitt 2006; Kobayashi and Weigel 2007; Michaels 2009), and the expression of floral repressors dampens responses to those cues delaying flowering. We use a previously developed flowering-time model that predicted the flowering behavior of multiple genotypes with 92% accuracy in diverse field conditions (Wilczek et al. 2009, 2010; Chew et al. 2012). We briefly outline this model and the equations below, but please see the above references for a more in-depth treatment.

Developmental progress toward flowering ($\text{MPTU}_{flowering}$) each hour (τ) is a multiplicative function of three factors: thermal(τ), photoperiod(τ), and floral repression(τ). Warm temperatures and long photoperiod increase development, whereas high floral repression levels reduce the number of modified photothermal units that accrue toward flowering.

The thermal component is given by

$$\text{thermal}(\tau) = \begin{cases} (T(\tau) - T_{b.f}) \times d_{hours} & \text{when } T(\tau) > T_{b.f} \\ 0 & \text{otherwise} \end{cases},$$

where T is temperature that hour, $T_{b.f}$ is the base temperature for flowering, and d_{hours} is a filter so that only thermal time that occurs during the daytime is included. The filter d_{hours} ranges in value from 0 (no light experienced that hour) to 1 (it is light for the whole hour).

The photoperiod component describes a broken stick model where developmental rate is divided into three sections. Rate is at a minimum (p_s) when the day length (D) is less than the critical short day length (d_s) and at a maximum (p_l) when D is above the critical long day length (d_l). In between d_s and d_l, developmental rate increases linearly from p_s to p_l:

$$\text{photoperiod}(\tau) = \begin{cases} p_s & \text{when } D(\tau) \leq d_s \\ p_s + \dfrac{(p_l - p_s) \times (D(\tau) - d_s)}{d_l - d_s} & \text{when } d_s < D(\tau) < d_l. \\ p_l & \text{when } D(\tau) \geq d_l \end{cases}$$

The floral repression component is given by a pair of nested equations. The first describes how winter chilling accumulates (WC_{sum}). Each hour, (τ) cold temperatures experienced are translated into winter chilling units via a beta function and are added to winter chilling accumulated in previous hours $\text{WC}_{sum}(\tau)$ until the requirement for winter chilling units is satisfied (WC_{sat}):

$$\text{WC}_{sum}(\tau + 1) = \begin{cases} \min\left(\text{WC}_{sum}(\tau) + e^{\kappa}(T(\tau) - T_{v.min})^{\omega} e^{\kappa}(T(\tau) - T_{v.max})^{\xi}, \text{WC}_{sat}\right) & \text{when } T_{v.min} \leq T(\tau) \leq T_{v.max} \\ \text{WC}_{sum}(\tau) & \text{otherwise} \end{cases},$$

where κ, ω, and ξ are fitted parameters determining the shape of the winter chilling–effectiveness function, and $T_{v.min}$ and $T_{v.max}$ are the minimum and maximum temperatures for winter chilling, respectively.

The second equation describes how the WC_{sum} state each hour is then used to determine floral repression levels. Here F_i is the initial floral repression level, and F_u is the ultimate level of repression after the winter chilling requirement (WC_{sat}) is satisfied:

$$\text{floral repression}(\tau) = \begin{cases} 1 - F_i + (F_i - F_u) \times \left(\dfrac{\text{WC}_{sum}(\tau)}{\text{WC}_{sat}}\right) & \text{when } \text{WC}_{sum}(\tau) < \text{WC}_{sat} \\ 1 - F_u & \text{otherwise} \end{cases}.$$

These equations combine to determine the modified photothermal units for flowering ($\text{MPTU}_{flowering}$) that accrue each hour:

$$\text{MPTU}_{flowering}(\tau) = \text{thermal}(\tau) \times \text{photoperiod}(\tau) \times \text{floral repression}(\tau).$$

Ultimately, development is summed up (flowering$_{sum}$) from the time of germination (τ_{germ}) until the flowering threshold ($\Theta_{flowering}$) is reached. The flowering threshold is determined using methods in Wilczek et al. (2009):

$$\text{flowering}_{sum}(\tau_{germ}) = \sum_{\tau_{germ}=0}^{\text{flowering}_{sum}(\tau_{germ})=\Theta_{flowering}} \text{MPTU}_{flowering}(\tau).$$

Seed Dispersal Submodel

As there were no published data on *Arabidopsis thaliana* reproduction dynamics, we developed a simple model of the progress toward seed dispersal as a function of temperature. We chose a thermal function because the rate of grain production is often related to temperature in crop studies (Lawlor and Mitchell 2000; Ainsworth and Ort 2010). Seeds are released when they reach a developmental threshold that reflects the time it takes the first 10% of seeds to mature ($\Theta_{dispersal}$). We use this time point because measurements of complete plant senescence in chambers likely overestimate reproductive period based on our experience with *A. thaliana* in the field. In chambers, plants experience moderate temperatures and permissive moisture conditions unlike plants in the field. In practice, seasonal changes such as the dryness of summer will interrupt reproduction.

The rate of progress toward seed dispersal was modeled as a function of temperature, such that the rate of progress is proportional to the difference between the soil surface temperature (T) and a base temperature for dispersal ($T_{b.d}$). Rate of thermal progress toward seed dispersal (TU$_{seed\,dispersal}$) was modeled as a thermally dependent developmental accumulation above a base temperature (T_b):

$$\text{TU}_{seed\,dispersal}(\tau) = \begin{cases} T(\tau) - T_{b.d} & \text{when } T(\tau) > T_{b.d} \\ 0 & \text{otherwise} \end{cases}.$$

The higher temperatures are above $T_{b.d}$, the faster development occurs. Development is summed each hour from flowering ($\tau_{flowering}$) until plants reach the threshold ($\Theta_{dispersal}$):

$$\text{seed dispersal}_{sum}(\tau_{flowering}) = \sum_{\tau_{flowering}=0}^{\text{seed dispersal}_{sum}(\tau_{flowering})=\Theta_{dispersal}} \text{TU}_{seed\,dispersal}(\tau).$$

Our range of simulated average maturation lengths (fig. B17) corresponds well to the range of average reproduction lengths reported by Chiang et al. (2012) in a field experiment. Model parameters and threshold were determined based on fit-to-seed dispersal times measured in chamber conditions at 14°C, 20°C, and 25°C, respectively, with the Columbia genotype at a neutral photoperiod (L. T. Burghardt, unpublished data).

Creation of Environmental Inputs

Because the phenology models use hourly environmental inputs, we converted the available environmental data to that scale. We used temperature predictions from 20 years of a climate model to create temperature replicates that encapsulated year-to-year climate variability. For moisture data, we used monthly contemporary moisture statistics from WorldClim and created stochastic moisture profiles driven by monthly precipitation amount and number of precipitation events. We also calculated latitude-specific photoperiods. Replicates of these environmental series were generated by (1) randomly drawing temperature from the sample of years, (2) pairing those profiles with site-specific photoperiod, and (3) combining those with stochastic moisture profiles.

Photoperiod

Equations were used to calculate the time of dawn and dusk at each latitude and photoperiod length (Ham 2005).

Temperature

Twenty years (2001–2020) of daily maximum and minimum temperature data were extracted from the National Oceanic and Atmospheric Administration's Geophysical Fluid Dynamics Laboratory CM2.1 A1B X1 climate scenario from grid cells over each of the four focal sites (NOAA GFDL 2004; Delworth et al. 2006). We then interpolated those maximum and minimum daily temperatures to hourly measures and subsequently translated them from air to surface temperatures as outlined below. Further details can be found in Wilczek et al. (2010). These 20 years of hourly data are assembled at random with replacement when we create environments for model runs at each location.

Converting Daily Maxima and Minima to Hourly Temperatures

Conversions were modified from Cesaraccio et al. (2001):

$$T(\tau) = \begin{cases} c + \dfrac{a}{2}\cos\left(\pi + \dfrac{\tau - H_n}{H_m - H_n}\pi\right) & H_n \leq \tau \leq H_m \\ T_s + k\log_j L & H_m \leq \tau \leq H_s \,, \\ T_s + b\sqrt{\tau - H_s} & H_s \leq \tau \leq H_p \end{cases}$$

where τ is the current hour and H_n, H_m, and H_s are the time of dawn, daily maximum, and dusk of that day, respectively. The day's minimum and maximum temperatures are T_n and T_m, respectively; and T_p is the next day's minimum temperature:

$$H_m = H_n + x\sin\left(\dfrac{2\pi(w - y)}{365}\right) + z \text{ and } b = \dfrac{T_p - T_s}{\sqrt{H_p - H_s}}.$$

Additional intermediates included temperature at sunset (T_s), estimated as $T_s = T_m - s(T_m - T_p)$; c is the arithmetic mean of T_m and T_n; a is the amplitude of increase $T_m - T_n$; k is $T_m - T_s$; the logarithmic base j is $1 + H_s - H_m$; and $L = j - (\tau - H_m)$. Final parameter values were set to $x = 2.036391$, $y = 79.22015$, $z = 9.285504$, and $s = 0.227538$ based on fitting to hourly temperatures gathered at all four sites modeled here plus in Cologne, Germany.

Air to Ground Conversion

Surface temperature (T_g) in kelvins was simulated for each hour based on Kelvin air temperature (T_a) according to

$$T_g(\tau) = aW + cT_a + e\sin\left(\dfrac{2\pi t}{365} + f\right) + d,$$

where a, c, d, e, and f are parameters fit empirically using ground-level data from European weather stations at each of the four sites studied here as well as one in Cologne, Germany ($a = 0.004099$, $c = 0.920493$, $d = 22.466179$, $e = 21.861643$, and $f = 1.549941$). Value W (hour, day of year) is clear-sky irradiance as calculated in Ham (2005), and t is (fractional) time in days since midnight on January 1.

Moisture

Stochastic moisture profiles were generated for each site. We obtained site-specific monthly precipitation totals and rainy-day totals derived from the Climate Research Unit in East Anglia. Each hour, the chance of a rain event occurring was based on the number of rainy days given the site and month of the year. After each rain event, the soil dried hourly according to the equation $\Psi(\tau) = \Psi(\tau - 1) + [\Psi(\tau - 1)(d)/p_{(m,s)}]$, where decay ($d$) is a constant parameter and cumulative precipitation (p) is dependent on both site (s) and month (m). Therefore, the soil drying is scaled such that it occurs more slowly after rain events in months and locations where the total amount of precipitation in a month was higher.

   While these precipitation inputs are qualitatively different between the sites in an arguably valid way, they are unlikely to be quantitatively correct. For instance, to maintain generality, we held d constant across sites despite potential differences in soil that may influence soil-drying rates. While we sacrifice some accuracy with this simple method, it will be nearly impossible to get accurate, long-term surface-water potential levels across Europe, particularly as such parameters are soil type specific. In any event, we are primarily interested in how landscape differences in moisture, temperature, and photoperiod inputs interact. A sensitivity analysis of the decay parameter indicates that we get similar site-specific-model results up to a point, as the absolute moistness of the environment changes. Overall, germination takes longer to occur in drier soils, and therefore the time in which seeds germinate given a dispersal day is pushed later in the season as the decay parameter increases.
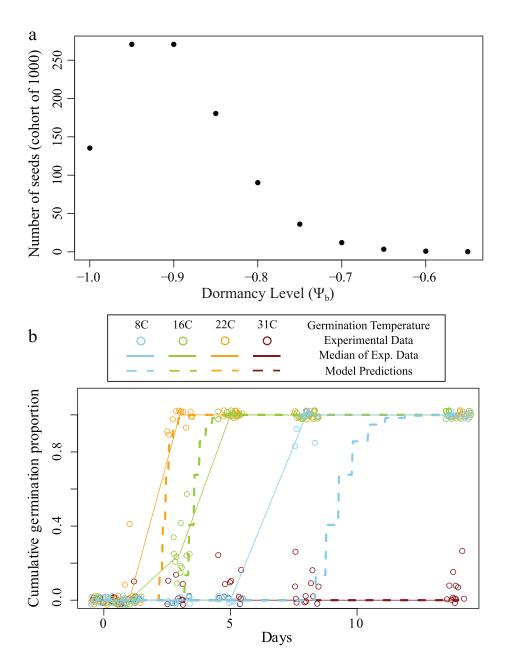
Figure A1: *a*, Poisson distribution of dormancy levels (Ψ_b used for germination model predictions). *b*, Germination model predictions superimposed over 12 replicated experimental time courses at each of four germination temperatures (8°, 16°, 22°, and 31°C). Circles show all replicates (note that these values are jittered on both the *X*- and *Y*-axes for visualization purposes). Solid lines show median germination at each time point, and dashed lines show model predictions. These seeds were 19 weeks old and represent 12 maternal replicate plants matured at 20°C in 12-h days.

Literature Cited Only in Appendix A

Ainsworth, E. A., and D. R. Ort. 2010. How do we improve crop production in a warming world? Plant Physiology 154: 526–530.

Bair, N. B., S. E. Meyer, and P. S. Allen. 2006. A hydrothermal after-ripening time model for seed dormancy loss in *Bromus tectorum* L. Seed Science Research 16:17–28.

Batlla, D., and R. L. Benech-Arnold. 2003. A quantitative analysis of dormancy loss dynamics in *Polygonum aviculare* L.

seeds: development of a thermal time model based on changes in seed population thermal parameters. Seed Science Research 13:55–68.

———. 2010. Predicting changes in dormancy level in natural seed soil banks. Plant Molecular Biology 73:3–13.

Bradford, K. J. 2002. Applications of hydrothermal time to quantifying and modeling seed germination and dormancy. Weed Science 50:248–260.

Carrera, E., T. Holman, A. Medhurst, D. Dietrich, S. Footitt, F. L. Theodoulou, and M. J. Holdsworth. 2007. Seed after-ripening is a discrete developmental pathway associated with specific gene networks in *Arabidopsis*. Plant Journal 53: 214–224.

Cesaraccio, C., D. Spano, P. Duce, and R. L. Snyder. 2001. An improved model for determining degree-day values from daily temperature data. International Journal of Biometeorology 45:161–169.

Chantre, G. R., M. R. Sabbatini, and G. A. Orioli. 2010. An after-ripening thermal-time model for *Lithospermum arvense* seeds based on changes in population hydrotime parameters. Weed Research 50:218–227.

Delworth, T. L., A. J. Broccoli, and A. Rosati. 2006. GFDL's CM2 global coupled climate models. Part I: formulation and simulation characteristics. Journal of Climate 19:643–674.

Finch-Savage, W. E., C. S. C. Cadman, P. E. Toorop, J. R. Lynn, and H. W. M. Hilhorst. 2007. Seed dormancy release in *Arabidopsis* Cvi by dry after-ripening, low temperature, nitrate and light shows common quantitative patterns of gene expression directed by environmentally specific sensing. Plant Journal 51:60–78.

Footitt, S., I. Douterelo-Soler, H. Clay, and W. E. Finch-Savage. 2011. Dormancy cycling in *Arabidopsis* seeds is controlled by seasonally distinct hormone-signaling pathways. Proceedings of the National Academy of Sciences of the USA 108:20236–20241.

Gutierrez, L., O. Van Wuytswinkel, M. Castelain, and C. Bellini. 2007. Combined networks regulating seed maturation. Trends in Plant Science 12:294–300.

Ham, J. M. 2005. Useful equations in micrometeorology. Pages 533–560 *in* J. L. Hatfield, J. M. Baker, and M. K. Viney, eds. Micrometeorology in agricultural systems. Vol. 47. American Society of Agronomy–Crop Science Society of America–Soil Science Society of America, Madison, WI.

Hardegree, S. P. 2006. Predicting germination response to temperature. I. Cardinal-temperature models and subpopulation-specific regression. Annals of Botany 97:1115–1125.

Hardegree, S. P., and S. S. Van Vactor. 1999. Predicting germination response of four cool-season range grasses to field-variable temperature regimes. Environmental and Experimental Botany 41:209–217.

Holdsworth, M. J., L. Bentsink, and W. J. J. Soppe. 2008. Molecular networks regulating *Arabidopsis* seed maturation, after-ripening, dormancy and germination. New Phytologist 179:33–54.

Iglesias-Fernández, R., M. del Carmen Rodríguez-Gacio, and A. J. Matilla. 2011. Progress in research on dry afterripening. Seed Science Research 21:69–80.

Kobayashi, Y., and D. Weigel. 2007. Move on up, it's time for change: mobile signals controlling photoperiod-dependent flowering. Genes and Development 21:2371–2384.

Lawlor, D. W., and R. A. C. Mitchell. 2000. Crop ecosystem responses to climatic change: wheat. Pages 57–80 *in* K. R. Reddy and H. F. Hodges, eds. Climate change and global crop productivity. CAB, New York.

Meyer, S. E., and P. S. Allen. 2009. Predicting seed dormancy loss and germination timing for *Bromus tectorum* in a semi-arid environment using hydrothermal time models. Seed Science Research 19:225.

Michaels, S. D. 2009. Flowering time regulation produces much fruit. Current Opinion in Plant Biology 12:75–80.

Mitchell-Olds, T., and J. Schmitt. 2006. Genetic mechanisms and evolutionary significance of natural variation in *Arabidopsis*. Nature 441:947–952.

NOAA GFDL (National Oceanic and Atmospheric Administration Geophysical Fluid Dynamics Laboratory). 2004. IPCC Fourth Assessment and US CCSP Projects. Princeton, NJ. http://data1.gfdl.noaa.gov.